On mesh bias of local damage models for concrete

Peter Grassl and Milan Jirásek
LSC, ENAC, Swiss Federal Institute of Technology at Lausanne (EPFL), Switzerland

1 INTRODUCTION

Quasibrittle materials, such as concrete, rock, tough ceramics, or ice, are characterized by the development of nonlinear fracture process zones, which can be macroscopically described as regions of highly localized strains. The degradation of strength and stiffness due to the progressive growth of microcracks and their coalescence is conveniently described by models based on continuum damage mechanics. If a standard (local) continuum theory is used, the softening part of the stress-strain law must be properly adjusted according to the size of the numerically resolved band of localized strain, which typically corresponds to the size of a finite element, or to a similar discretization parameter if another numerical technique is used. This adjustment eliminates the pathological dependence of the solution on the finite element mesh and ensures that the global energy dissipation in the failure process is captured correctly. However, the results of the numerical simulation can still be polluted by mesh-induced directional bias which, in some cases, may lead to wrong failure mechanisms and to a misprediction of the ultimate load.

In the present comparative study, we investigate the influence of mesh bias on failure simulations performed with isotropic and anisotropic damage models. Two isotropic formulations are considered, one with the Rankine and the other with the modified von Mises strength envelope. As a representative anisotropic damage model, the microplane-based damage model (MDM) developed in the past by the second author is considered. Several fracture tests with curved crack trajectories are simulated on different meshes, and general conclusions are drawn based on the evaluation of the numerical results. Finally, a crack tracking technique (inspired by embedded crack models but implemented here for continuum damage models) is proposed, and a substantial reduction of mesh bias obtained with this approach is demonstrated.

2 DAMAGE MODELS

2.1 Isotropic damage

The simple isotropic damage model considered here is described by the basic equations

$$\boldsymbol{\sigma} = (1-\omega)\boldsymbol{D}_e : \boldsymbol{\varepsilon} \qquad (1)$$

$$\omega = g(\kappa) \qquad (2)$$

$$f(\boldsymbol{\varepsilon},\kappa) \leq 0, \qquad \dot{\kappa} \geq 0, \qquad \dot{\kappa}f(\boldsymbol{\varepsilon},\kappa) = 0 \quad (3)$$

in which $\boldsymbol{\sigma}$ is the stress tensor, $\boldsymbol{\varepsilon}$ is the strain tensor, $\boldsymbol{D}_e$ is the elastic stiffness tensor, ω is a scalar damage variable, κ is an internal variable that drives damage, and f is the damage loading function. The typical form of the loading function is

$$f(\boldsymbol{\varepsilon},\kappa) = \tilde{\varepsilon}(\boldsymbol{\varepsilon}) - \kappa \qquad (4)$$

where $\tilde{\varepsilon}$ is a scalar measure of the current strain level called the equivalent strain. The internal variable κ has then the physical meaning of the maximum value of equivalent strain ever reached in the previous history of the material up to the current state.

The choice of a specific expression for the equivalent strain $\tilde{\varepsilon}$ determines the shape of the elastic domain and depends on the type of material. For tensile-dominated failure of quasibrittle materials, one possible choice is

$$\tilde{\varepsilon} = \frac{1}{E}\sqrt{\langle\boldsymbol{\sigma}_e\rangle : \langle\boldsymbol{\sigma}_e\rangle} = \frac{1}{E}\sqrt{\sum_{I=1}^{3}\langle\sigma_{eI}\rangle^2} \qquad (5)$$

where $\boldsymbol{\sigma}_e = \boldsymbol{D}_e : \boldsymbol{\varepsilon}$ is the effective stress tensor, σ_{eI}, $I = 1,2,3$, are its principal values, and $\langle\ldots\rangle$ is the positive part operator. Definition (5) leads to a Rankine-type strength envelope with a smooth round-off in the sectors of two or three positive principal stresses; see Figure 1. A recently proposed alternative formula,
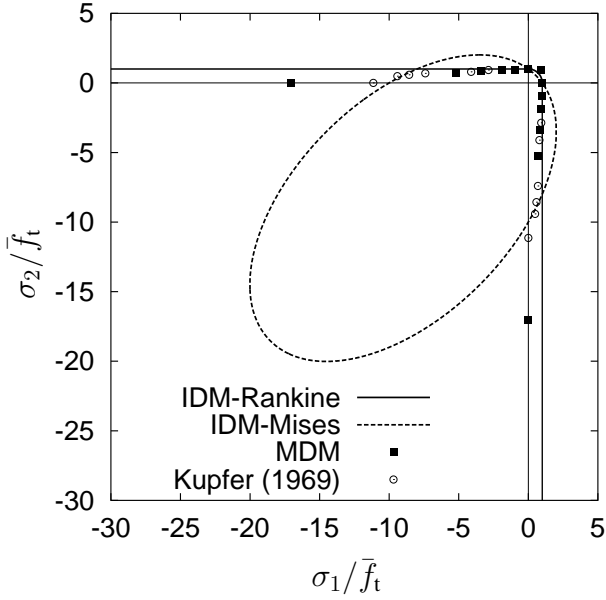
Figure 1: Biaxial strength envelope for different damage models and experimental data.

called the modified von Mises definition (de Vree, Brekelmans, and van Gils 1995), reads

$$\tilde{\varepsilon} = \frac{k-1}{2k(1-2\nu)}I_1 + \frac{1}{2k}\sqrt{\frac{(k-1)^2}{(1-2\nu)^2}I_1^2 - \frac{12k}{(1+\nu)^2}J_2} \tag{6}$$

where

$$I_1 = \varepsilon_{kk} J_2 = \frac{1}{6}I_1^2 - \frac{1}{2}\varepsilon_{ij}\varepsilon_{ij} \tag{7}$$

is the first invariant of the strain tensor,

$$J_2 = \frac{1}{6}I_1^2 - \frac{1}{2}\varepsilon_{ij}\varepsilon_{ij} \tag{8}$$

is the second invariant of the deviatoric strain tensor, ν is the Poisson ratio, and k is the ratio between the uniaxial compressive strength $\bar{f}_c$ and uniaxial tensile strength $\bar{f}_t$.

The function g, which relates the damage variable ω to the internal variable κ according to (2), is assumed to have the exponential form

$$g(\kappa) = \begin{cases} 0 & \text{if } \kappa \leq \varepsilon_0 \\ 1 - \frac{\varepsilon_0}{\kappa}\exp\left(-\left(\frac{\kappa-\varepsilon_0}{\varepsilon_f-\varepsilon_0}\right)\right) & \text{if } \kappa \geq \varepsilon_0 \end{cases} \tag{9}$$

where ε_0 is the strain at peak stress under uniaxial tension, and ε_f is a parameter that controls the slope of the softening curve (Figure 2), which can be related to the fracture energy G_F and to the finite element size.

2.2 *Anisotropic damage*

The anisotropic damage model considered in this study is based on the principle of energy equivalence (Cordebois and Sidoroff 1979) and on the theoretical framework proposed by Carol and Bažant (1997) in
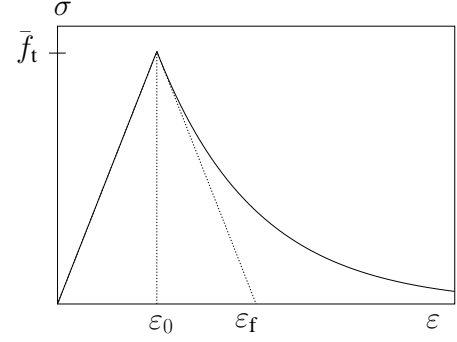

Figure 2: Uniaxial stress-strain curve with exponential softening.

the context of the microplane damage theory. A specific version of this model was developed by Jirásek (1999) and is called the microplane based damage model (MDM).

3 COMPARATIVE STUDY

To assess the directional mesh bias in finite element simulations with local damage models, three fracture tests were analyzed using three different models, each time on triangular and quadrilateral meshes. The models included in the study are

- the isotropic damage model with Rankine-type definition of equivalent strain (IDM-Rankine),

- the isotropic damage model with modified von Mises definition of equivalent strain (IDM-Mises), and

- the anisotropic damage model based on the principle of energy equivalence and the microplane theory (MDM).

3.1 *Four-point shear test*

The first example is a four-point shear test of a single-edge-notched (SEN) beam tested by Arrea and Ingraffea (1982). The geometry with the loading setup and the crack trajectories obtained in the experiments are shown in Figure 3.
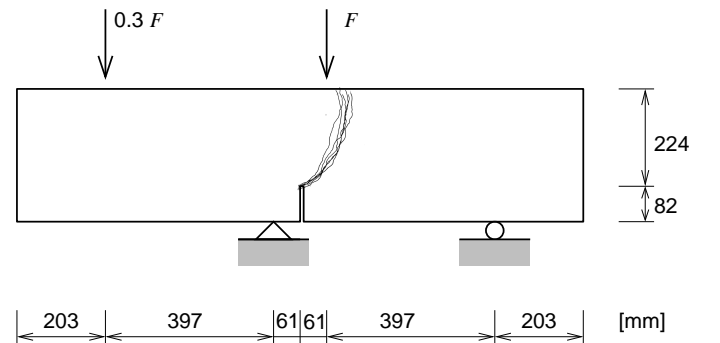

Figure 3: Four-point shear test: Experimental setup and crack trajectories.
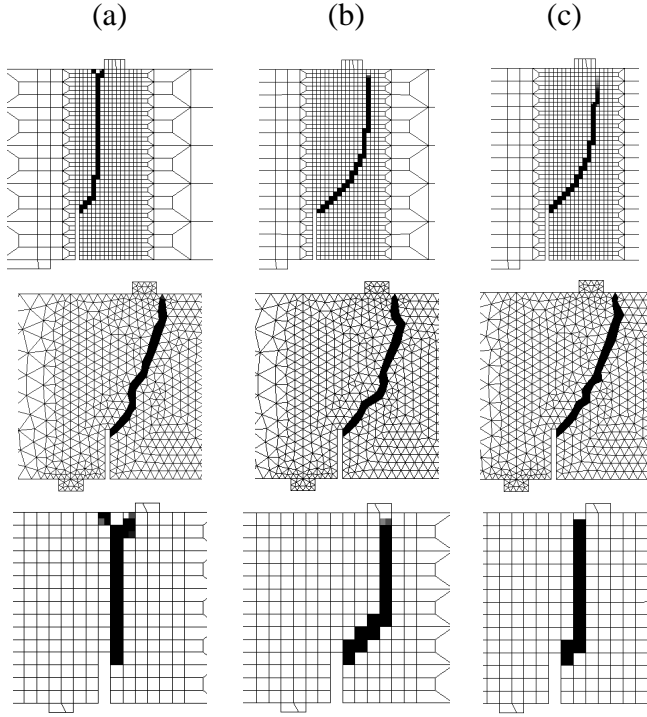
2

Figure 4: Influence of mesh size and element type on the crack band trajectory in the four-point shear test for (a) IDM-Rankine, (b) IDM-Mises and (c) MDM.

The material parameters were chosen for all models as follows: Young's modulus $E = 30$ GPa, Poisson's ratio $\nu = 0.18$, tensile strength $\bar{f}_t = 3.5$ MPa, and fracture energy $G_F = 140$ J/m^2. For the IDM-Mises model, the ratio between the compressive and tensile strength, $k = \bar{f}_t/\bar{f}_c$, was set to 10, and for the MDM model, the parameter m_d that controls sensitivity to the confining pressure was set to 0.05.

Three different finite element meshes were used:

- fine structured mesh of bilinear quadrilateral elements with four integration points,

- fine unstructured mesh of constant-strain triangular elements with one integration point, and

- coarse structured mesh of bilinear quadrilateral elements with four integration points.

The simulated crack trajectories are shown in Figure 4. The dark elements are those with a high level of maximum principal strain (exhibiting at the same time a high level of damage).

3.2 *Double-edge-notched specimen*

The second example is the double-edge-notched (DEN) specimen tested by Nooru-Mohamed (1992). The experimental setup is shown in Figure 5a. The nonproportional loading path 4c was chosen for the comparison. This is the most challenging test of the
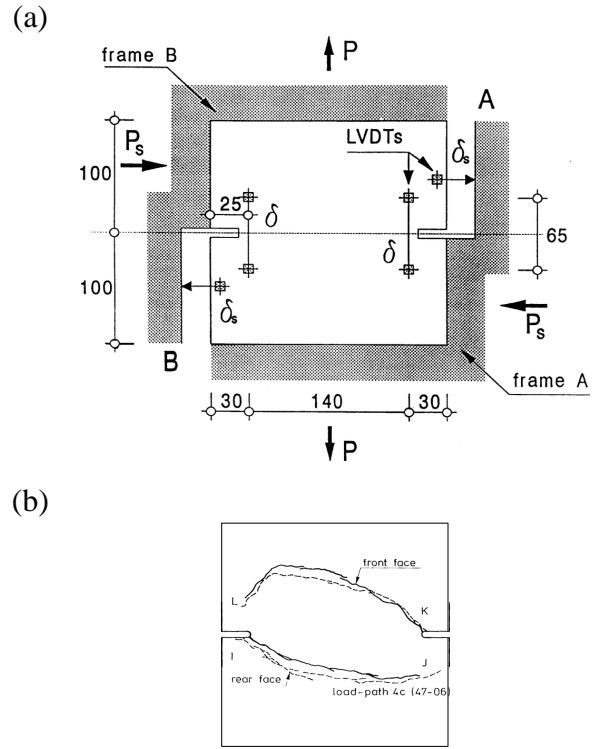

Figure 5: The DEN specimen: (a) geometry and loading, (b) observed crack pattern for loading path 4c (after Nooru-Mohamed 1992).
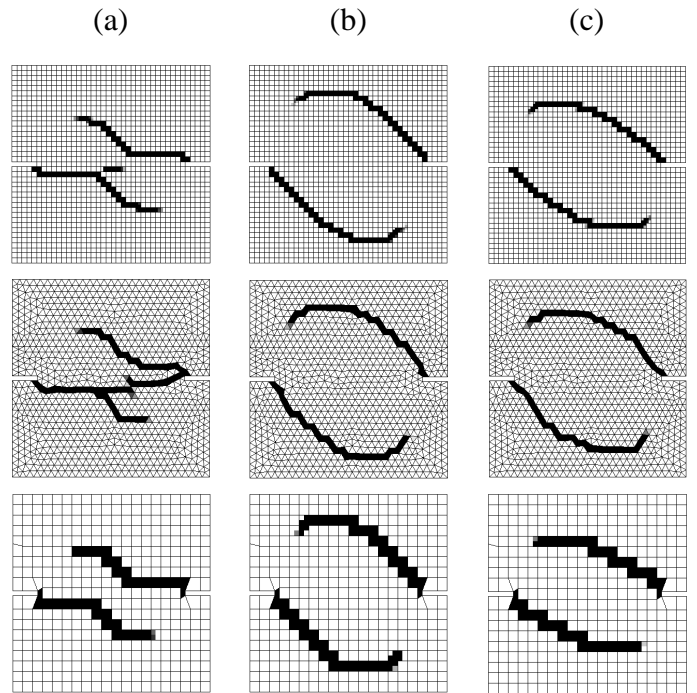

Figure 6: Influence of mesh type and element size on the crack band trajectory in the DEN test for (a) IDM-Rankine, (b) IDM-Mises and (c) MDM.
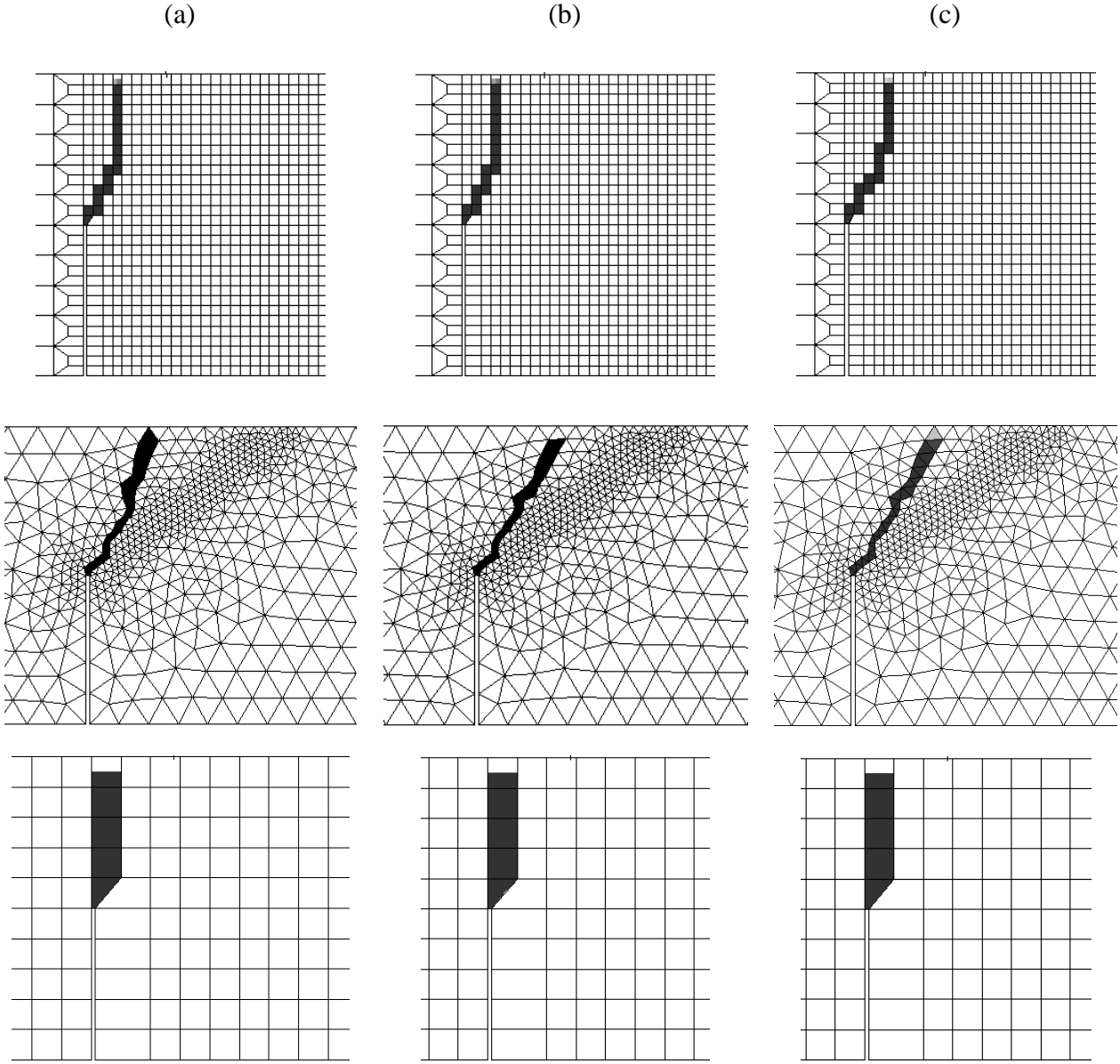
3

Figure 7: Influence of mesh type and element size on the crack band trajectory in the nonsymmetric three-point bending test ($K = 0$) for (a) IDM-Rankine, (b) IDM-Mises and (c) MDM.

entire testing program, because the final failure pattern consists of two cracks with a relatively strong curvature; see Figure 5b. During the first stage, the specimen is loaded by an increasing "shear" force, P_s, until the maximum force that the specimen can carry is reached. Then, in the second stage, this force is kept constant and a "normal" force, P, is applied in the vertical direction.

The material parameters were chosen as $E = 29$ GPa, $\nu = 0.2$, $f_\mathrm{t} = 3$ MPa, $G_\mathrm{F} = 110$ J/m^2, $k = 10$ for the IDM-Mises and $m_\mathrm{d} = 0.05$ for the MDM model. Again, three types of finite element meshes were used. The failure patterns are presented in Figure 6.
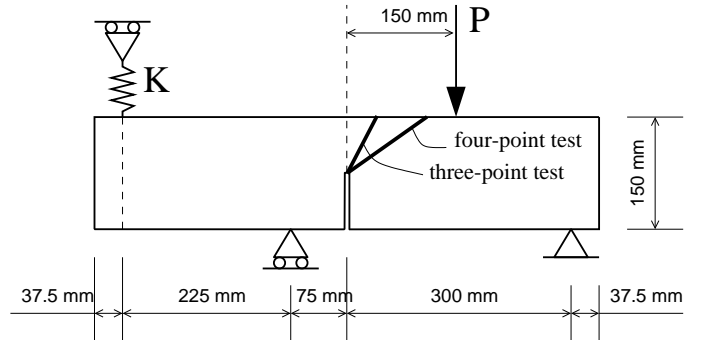

Figure 8: Nonsymmetric bending tests: Geometry and loading with mean crack paths observed in experiments.
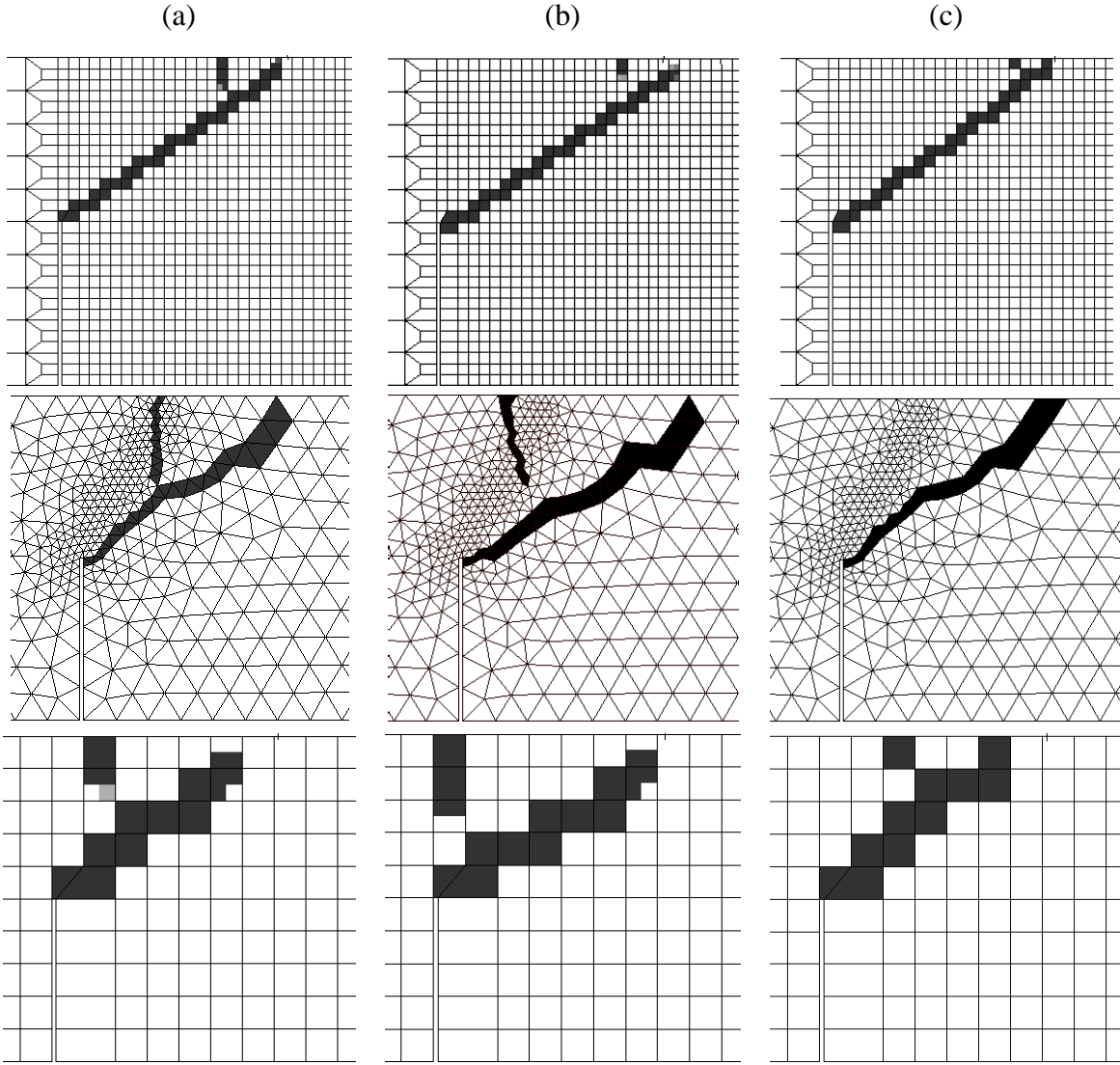
4

(a)   (b)   (c)

Figure 9: Influence of mesh size and element type on the crack band trajectory in the four-point bending test ($K = \infty$) for (a) IDM-Rankine, (b) IDM-Mises and (c) MDM.

3.3 *Nonsymmetric bending tests*

The third example presents the three- and four-point bending tests reported by Galvez et al. (1998). The test geometry and the loading setup are shown in Figure 8. For a spring stiffness value of $K = 0$ the test setup results in a nonsymmetric three-point bending test, whereas for $K = \infty$ a nonsymmetric four-point bending test is obtained. In the two tests two crack paths of different orientations were obtained, running approximately along the straight lines shown in Figure 8.

The experiments were simulated on three different meshes: two quadrilateral meshes (fine and coarse) analogous to the previous two tests, and a triangular mesh deliberately misaligned with the experimentally observed crack paths. The failure patterns for the analyses with $K = 0$ (three-point bending) and $K = \infty$ (four-point bending) are shown in Figures 7 and 9.

3.4 *Discussion of the results*

The **isotropic** damage model with the **Rankine**-type expression for equivalent strain (5) is in general strongly sensitive to the mesh orientation. In the four-point shear test reported in Section 3.1, the simulated crack trajectories are strongly attracted by the mesh lines. For the structured quadrilateral meshes, the crack ends on the left side of the upper support, which is not in agreement with the crack trajectories observed in the tests; see Figure 3. For the DEN test in Section 3.2, the results are even worse. Here, the IDM-Rankine cannot represent the curved crack trajectories obtained in the experiments. Even the straight crack trajectory of the nonsymmetric three-point bending testreported in Section 3.3 is not reproduced because the pattern of localized strain is influenced by the vertical mesh lines. The straight crack of the nonsymmetric four-point bending test is well captured, but the failure pattern is disturbed by a spurious
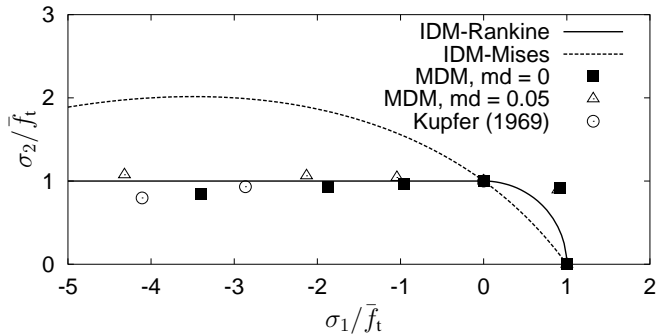
Figure 10: Detail of the strength envelope in region of biaxial tensile-compressive stress states.

secondary crack.

The results obtained with the **isotropic** damage model improve if the equivalent strain is computed according to the modified von **Mises** definition (6). The simulated crack trajectories in the first two examples appear to be almost independent of the mesh alignment and refinement. This is not the case in the nonsymmetric bending tests (Section 3.3). For the three-point bending test, the pattern of localized strains is influenced by the mesh lines. For the four-point bending test, spurious secondary crack appears.

The strikingly different results obtained with the IDM-Rankine and IDM-Mises in the four-point shear and DEN tests might seem surprising, since both models are isotropic and only differ in the type of loading function. The explanation for this strong difference is found in the shape of the failure surface in the region of biaxial tensile-compressive stress states.

For the Rankine-type definition of equivalent strain, the maximum tensile stress in the biaxial tension-compression region is equal to the uniaxial tensile strength. On the other hand, for the modified von Mises definition, the maximum tensile stress under biaxial tension-compression is up to twice the uniaxial tensile strength; see Figure 10.

In the first two experiments, the curved crack propagates in a compressive stress field. For the IDM-Rankine, the compressive stress does not influence the tensile strength, and the mesh alignment has a strong influence on the crack trajectory. On the contrary, the IDM-Mises has a greater tensile strength in the presence of compressive stresses parallel to the crack, and this forces the numerical crack to propagate "around" the compressive strut. For this reason, the curved crack path observed in the experiments is reproduced independently of the orientation of the mesh. However, the increase of tensile strength in biaxial tension-compression stress state is artificial, because it does not correspond to experimental data.

The strength envelope of concrete under biaxial stress was determined, for instance, in the experimental study by Kupfer et al. (1969). It was found that under biaxial tension-compression the tensile strength slightly decreases with increasing compressive stresses in the perpendicular direction. The artificial increase of the tensile strength for biaxial tension-compression exhibited by the IDM-Mises model may lead in other examples, in which the strength in biaxial tension and compression is decisive, to an overestimation of the load resistance.

For the **anisotropic** MDM model, the exact shape of the biaxial strength envelope depends on parameter m_d, but this dependence is quite weak. The best agreement with Kupfer's data is achieved for $m_d = 0$, but even with the default value $m_d = 0.05$ the numerical strength envelope remains close to the experimental one; see Figure 10.

The MDM model, as a representative anisotropic damage model, gives on fine meshes (both structured and unstructured ones) good predictions of the crack trajectories in almost all the tests The only exception is the nonsymmetric three-point bending test, for which the mesh bias affect a part of the crack trajectory simulated on a fine quadrilateral mesh, but the result is still slightly better than with the isotropic models. Spurious secondary cracking in the four-point bending test appears only on the coarse mesh. In the three-point bending and four-point shear tests, the results on coarse meshes suffer by the directional bias, but the Nooru-Mohamed test of the DEN specimen is reasonably well reproduced even on the coarse mesh.

4 THE CRACK TRACKING METHOD

The crack tracking method is a newly proposed technique that can overcome the dependency of isotropic damage models on the mesh orientation. It combines a tracking algorithm, as known from the strong discontinuity approach (Jirásek and Zimmermann 2001), with an isotropic damage model based on the smeared crack concept.

The main idea is that the localized process zone is described not only by a band of damaged elements, but also by its idealized centerline, approximated by a sequence of contiguous straight segments. The first segment is placed in the center of the first cracking element and is extended to the boundaries of that element. The direction of the segment is determined from the weighted average of strain in the neighborhood of the integration point at the element center, and is taken as perpendicular to the principal direction corresponding to the maximum principal value of the averaged strain tensor. The intersections of the segment with the element boundaries define at most two computational crack tips. Often, the first crack-
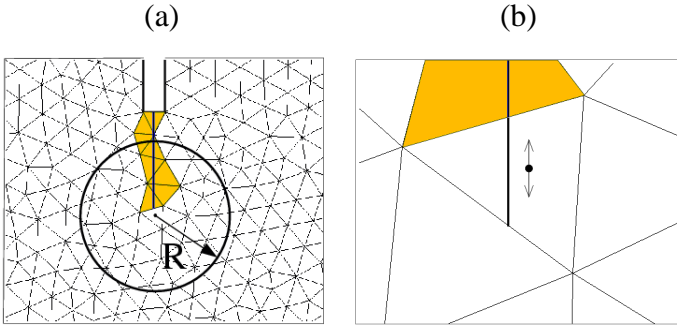
6

(a)   (b)

Figure 11: Propagation of crack band centerline: (a) determination of the direction of the new crack segment from the weighted average of the strain over a neighborhood of radius R, (b) extension of the centerline by a new segment and determination of the new crack tip.
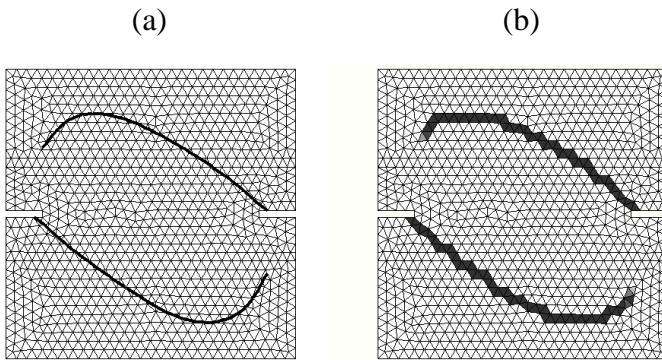
(a)   (b)

Figure 12: (a) Crack trajectory obtained by the tracking method in the DEN test, and (b) the corresponding bands of elements with localized strain.

ing element is adjacent to the physical boundary of the specimen and one of these "tips" is actually the crack mouth. The position of the other tip defines the element that is "to be entered by the crack".

In subsequent loading steps, damage is allowed to grow only in the elements already crossed by a crack segment, element to be entered by the crack, or elements that are sufficiently far from the previously mentioned ones (to allow the formation of another process zone in a different part of the specimen).

As shown in Figure 11, a new crack segment is added to the already existing ones when the equivalent strain at the integration point of the element in front of the crack tip reaches a critical level. The new segment starts at the current crack tip and is perpendicular to the principal direction of the averaged strain tensor corresponding to the maximum principal value. The intersection of the segment with the element boundary defines the new position of the crack tip and the neighboring element that is the next candidate for cracking.

The crack tracking technique permits a better resolution of the failure pattern, which is less sensitive to the directional mesh bias. This is documented in Figure 12, showing the sequence of crack segments and the corresponding bands of damaged elements for the Nooru-Mohamed DEN test from Section 3.2. The simulation used the isotropic damage model with Rankine-type expression (5) for equivalent strain. Without the crack tracking technique, the failure pattern would be completely mispredicted; see Figure 6a.

5 CONCLUSIONS

The evaluation of mesh-induced directional bias of two isotropic and one anisotropic damage model on different types of meshes for a number of concrete fracture tests has lead to the following preliminary conclusions:

- The isotropic damage model with a realistic biaxial strength envelope is strongly sensitive to the mesh orientation, even if the mesh is fine.

- The isotropic damage model with a modified von Mises definition of equivalent strain appears to be less sensitive to the mesh orientation, but this is to a large extent an artifact caused by the unrealistic increase of tensile strength under compression parallel to the crack.

- The anisotropic damage model used in this study can reasonably well capture arbitrary crack trajectories, while the biaxial strength envelope remains close to typical experimental data for concrete.

- Mesh refinement often reduces sensitivity to the mesh orientation, but is not a universal remedy.

These conclusions need to be confirmed by further investigations. In particular, alternative anisotropic models such as the rotating crack model should be included in the comparative study, to see whether anisotropy is indeed the key to mesh bias reduction.

The isotropic damage model is attractive for its simplicity but, with a definition of equivalent strain that provides a realistic biaxial strength envelope, it is strongly sensitive to the mesh orientation. Modification of the equivalent strain definition is not a physically sound remedy, as discussed before. As an alternative technique aiming at the reduction of mesh bias, the crack tracking method has been proposed in the present paper. This method is based on the tracking of the crack centerline and can be combined with any standard constitutive model and two-dimensional finite element. The crack tracking method is able to simulate the crack patterns of complex mixed-mode fracture tests using a simple isotropic damage model with a Rankine loading function. A substantial improvement has been observed in the Nooru-Mohamed

DEN test, but a more extensive evaluation of the true potential of this method is needed.

REFERENCES

Arrea, M. and A. R. Ingraffea (1982). Mixed-mode crack propagation in mortar and concrete. Department of Structural Engineering 81-83, Cornell University, Ithaca, NY.

Carol, I. and Z. P. Bažant (1997). Damage and plasticity in microplane theory. *International Journal of Solids and Structures 34*, 3807–3835.

Cordebois, J. P. and F. Sidoroff (1979). Anisotropie élastique induite par endommagement. In *Comportement mécanique des solides anisotropes*, Number 295 in Colloques internationaux du CNRS, Grenoble, pp. 761–774. Editions du CNRS.

de Vree, J. H. P., W. A. M. Brekelmans, and M. A. J. van Gils (1995). Comparison of nonlocal approaches in continuum damage mechanics. *Computers and Structures 55*, 581–588.

Galvez, J. C., M. Elices, G. V. Guinea, and J. Planas (1998). Mixed mode fracture of concrete under proportional and nonproportional loading. *International Journal of Fracture 94*, 267–284.

Jirásek, M. (1999). Comments on microplane theory. In G. Pijaudier-Cabot, Z. Bittnar, and B. Gérard (Eds.), *Mechanics of Quasi-Brittle Materials and Structures*, Paris, pp. 55–77. Hermès Science Publications.

Jirásek, M. and T. Zimmermann (2001). Embedded crack model: II. Combination with smeared cracks. *International Journal for Numerical Methods in Engineering 50*, 1291–1305.

Kupfer, H., H. K. Hilsdorf, and H. Rüsch (1969). Behavior of concrete under biaxial stresses. *Journal of the American Concrete Institute 66*, 656–666.

Nooru-Mohamed, M. B. (1992). *Mixed-mode fracture of concrete: An experimental approach*. Ph. D. thesis, Delft University of Technology, The Netherlands.

Patzák, B. (1999). Object oriented finite element modeling. *Acta Polytechnica 39*, 99–113.

Patzák, B. and Z. Bittnar (2001). Design of object oriented finite element code. *Advances in Engineering Software 32*, 759–767.